IJAME
Int. J. of Applied Mechanics and Engineering, 2025, vol.30, No.1, pp.18-37
DOI: 10.59441/ijame/210538

TRANSIENT MAGNETO-CONVECTION OF WATER NEAR ITS MAXIMUM DENSITY IN A CAVITY WITH VARIOUS SINK-SOURCE ARRANGEMENTS AND HEAT GENERATION

R. Bindhu[1], S. Sivasankaran[2] and K.K. Viswanathan[3*]
[1]Department of Mathematics, PSG College of Technology, Coimbatore, INDIA
[2]Department of Mathematics, King Abdulaziz University, Jeddah, SAUDI ARABIA &
Saveetha School of Engineering, SIMATS, Chennai, INDIA
[3]Department of Mathematical Modeling, Samarkand State University, UZBEKISTAN &
University of Economics and Pedagogy, Karshi, UZBEKISTAN
E-mail: visu20@yahoo.com

This study emphasizes the transient and steady state analysis on magneto-convection of cold water driven by buoyant force in a chamber with partial heating and cooling combined with internal heat absorption/generation. The considered cavity is of square geometry bounded with different locations of source-sink pairs along its left and right sides. The analysis is confined by placing the source-sink pairs to five different locations traversing in the vertical direction along the boundary. The discretization is implemented using a finite volume approach. QUICK scheme and central difference schemes are utilized to resolve the convective and diffusive terms respectively. The SIMPLE algorithm is implemented to ensure the relation of pressure-velocity term. Gauss-Seidel iterative process is applied to find the unknowns from the resulting set of equations. Out of the five cases analyzed, Case 5 (TB) demonstrated a higher transfer rate, while Case 4 (BT) exhibited a lower heat transmission rate in the presence of heat generation or absorption. When heat generation/absorption was absent, Case 2 (MM) showed an improved heat transfer rate. The findings can be applied in industries such as electronic cooling devices, solar collectors, and thermal energy storage systems.

Key words: maximum density, source-sink location, MHD, free convection, heat generation.

1. Introduction

The convective movement and thermal transfer in chambers with partially/discreetly heated or cooled vertical walls with internal heat generation has gained special attention due to its numerous applications in engineering and technology [1-2]. The study on internal heat generation / absorption is very significant since its effects alter the temperature distribution in the fluid [3-4]. Consequently understanding its effects in physical problems has become very vital. Also, great interest is shown in studying the fluids inside enclosures since many thermal systems include enclosures in it. Another important aspect to be considered is the common use of water as a coolant. Mostly, thermal storage devices use water as a working fluid because of its nontoxic nature and easy availability. Touiker *et al.* [5] explored the thermo-solutal convection in a chamber with (hot) source immerged in a porous medium. They obtained the optimum location of the heat source for best thermal transport. Rahimi *et al.* [6] conducted studies on lattice Boltzmann simulations of natural convective movement in a chamber with active hot and cold portions on sidewalls, as well as internal hot/cold obstacles. Patterson [7] examined unsteady buoyant convection in a closed chamber with internal heating and cooling. Baytas [8] carried out a computational study on buoyancy-driven stream in a closed domain with time-periodic internal heat sources. Tasaka and Takeda [9] scrutinized the consequence of heat source distribution on buoyant convection induced by internal heating. Hossain *et al.* [10] investigated thermo-capillary and buoyancy driven convection of an electrically conducting liquid within a chamber with heat absorption/generation. They concluded that heat generation plays a vital role

* To whom correspondence should be addressed

in the development of multiple cells inside the chamber. Saravanan *et al.* [11] investigated natural convection within a square enclosure driven by two thin, heated plates positioned at arbitrary locations and oriented perpendicularly. Their study compared isothermal and isoflux boundary conditions, revealing that isothermal boundaries produced a more pronounced convection pattern. Hakeem *et al.* [12] showed the influence of heat-generating baffles placed within the chamber. Their findings indicated that the positioning of the baffles significantly influenced both the flow dynamics and temperature distribution.

Unlike the other fluids, water has its maximum density about $4°C$ and this complicates the flow pattern and heat transfer. This interesting phenomenon motivates investigators to study further in this area and so several analyses are carried out during the past decades and were analyzed both numerically and experimentally by Ho and Tu [13]. Hossain and Rees [14] investigated numerically the convective flow of water near its maximum density in a cavity having isothermal walls and internal heat generation. It was found that the flow and temperature field strongly depend on internal heat generation parameter and when the generation is strong the circulation of the flow is reversed. The effects of temperature dependent properties of cold water around its maximum density in the occurrence of uniform (external) magnetic field were studied by Sivasankaran and Ho [15]. The consequences of volumetric heat source on free convection in wavy enclosures were deliberated numerically by Oztop *et al.* [16]. They disclosed that both the stream and thermal features were affected by changing the Rayleigh number ratio and wavy wall's amplitude.

The study on electrically conducting fluids becomes highly significant due to its versatile interdisciplinary applications specified by Hiremath *et al.* [17], Sahoo and Rathish Kumar [18], and Gangawane and Bharti [19]. Engineering problems like liquid metal cooling of nuclear reactors, plasma confinement, working of magneto hydrodynamic pumps etc., are analyzed and improved with the ideas of MHD properties in the works finished by Beg *et al.* [20], Prasad *et al.* [21], and Joshi *et al.* [22]. In large reactors, especially the advanced nuclear reactors used today, utilize only liquid metal as its coolant in the place of water to remove the heat produced inside the system. This is due to the fact that flow rate of liquid water gets attenuated by the occurrence of magnetic field and internal heat (absorption) generation within the system. This in turn deteriorates the heat transmission rate. However, due to easy availability of water resource, study on natural convective stream of (cold) water under the influence of magnetic field in enclosures gains high interest among researchers. Saravanan *et al.* [23] examined the impact of isothermal or isoflux heating conditions on magneto-convection in a cavity with partial heating from a heat source located on the bottom wall. Sivasankaran *et al.* [24] deliberated the consequence of an external (uniform) magnetic field and divider on natural convection in a chamber. They detected that the rate of heat transmission gains with increase of Grashof number and Prandtl number for both cases of partition (vertical and horizontal).

Sivasankaran and Bhuvaneswari [25] numerically investigated the outcome of orientation of external (uniform) magnetic field strength and partially active zones on natural convective stream in a chamber. Malleswaran *et al.* [26] explored the outcome of locality and size of heater on magneto-convection in a lid-driven chamber. Benos *et al.* [27] designed analytical and numerical research of MHD free convection in a shallow horizontal cavity with heat generation. They demonstrated that the liquid flow is slowed by the magnetic field effect. This deceleration leads to the dominance of (heat) conduction and to the reduction of thermal transport. Janagi *et al.* [28] calculated the effects of buoyant convection of water about $4℃$ in a square porous cavity. They identified that the increase of density inversion factor decreases the convective heat transmission rate firstly and then increases. Das and Basak [29] examined the various discrete heating effect strategies along vertical walls inside the porous cavities with triangular and square geometry subjected to heater locations that are symmetric and asymmetric.

Many researchers in the past literature have studied the problem of natural (mixed) convection in cavities with partial cooling/heating. However, investigations on this attenuating effect of cold water around its supreme density in the occurrence of internal heat generation and (external) magnetic field are reported less. This has inherently motivated this work and so here, analysis is carried out numerically to study the pattern of stream and thermal transfer that happens inside an enclosure with partially heated/cooled walls for several values of internal heat generation around density extreme of water in the occurrence of magnetic field. Also, ideal values for heat generation parameter and magnetic field are identified in this study where an effective and enhanced heat transfer can take place.

2. Modeling and formulation

The physical configuration taken under consideration is a 2-dimensional square enclosure of height H_E filled with cold water as presented in Fig.1. A segment of length $H_E / 2$ on both the right and the left walls is maintained at a temperature T_c and T_h respectively with $T_c < T_h$. The remaining area of walls of the chamber are kept insulated. It is assumed that the flow is unsteady and laminar. The fluid is incompressible. The five different sink-source pairs along the vertical walls are studied here. That is, the hot source and cold sink are placed along the vertical walls and are placed at three different locations namely the top, center and bottom. That is, they are placed along the top portion of walls referred as case 1 (TT). The center locations are referred as case 2 (MM) and bottom arrangements referred as case 3 (BB). The source at bottom of left wall and sink at top of right all referred as case 4 (BT). Similarly, the source at top of left wall and sink at bottom of right all referred as case 5 (TB). It is presumed that the uniform external magnetic field of strength B_0 is applied parallel to $x-$axis and the induced magnetic field is insignificant. The density variations of water follow the relation $\rho = \rho_m 1 - \beta_T \left|T - T_m\right|^b$ where β_T being thermal expansion coefficient [11]. The subscript m indicates the density inversion state and the Boussinesq approximation holds good for the mathematical formulation. Also, the viscous dissipation is not taken here.

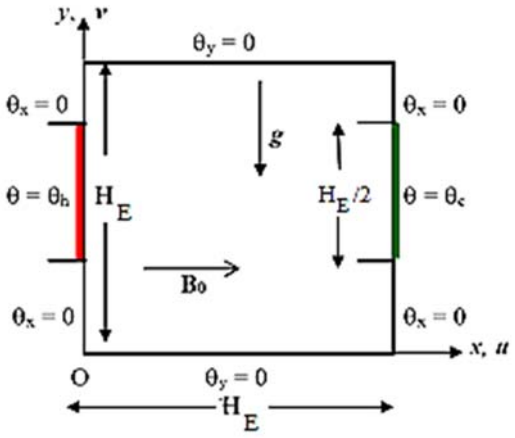

Fig.1. Physical model and boundary conditions.

With the above taken assumptions, the unsteady two-dimensional equations governing the model are as follows [13, 25, 28]:

$$\frac{\partial u}{\partial x} + \frac{\partial v}{\partial y} = 0, \tag{2.1}$$

$$\frac{\partial u}{\partial t_0} + u\frac{\partial u}{\partial x} + v\frac{\partial u}{\partial y} = -\frac{1}{\rho_0}\frac{\partial p}{\partial x} + \upsilon\left[\frac{\partial^2 u}{\partial x^2} + \frac{\partial^2 u}{\partial y^2}\right], \tag{2.2}$$

$$\frac{\partial v}{\partial t_0} + u\frac{\partial v}{\partial x} + v\frac{\partial v}{\partial y} = -\frac{1}{\rho_0}\frac{\partial p}{\partial y} + \upsilon\left[\frac{\partial^2 v}{\partial x^2} + \frac{\partial^2 v}{\partial y^2}\right] + g\beta\left|T - T_m\right|^b - \frac{\sigma_e B_0^2 v}{\rho_0}, \tag{2.3}$$

$$\frac{\partial T}{\partial t_0} + u\frac{\partial T}{\partial x} + v\frac{\partial T}{\partial y} = \frac{k}{\rho_0 c_p}\left[\frac{\partial^2 T}{\partial x^2} + \frac{\partial^2 T}{\partial y^2}\right] + \frac{q'''(T - T_c)}{\rho_0 c_p} \tag{2.4}$$

where $u, v, p, T, \nu, \rho_0, k, \sigma_e, \beta, q''', c_p$ represent the x and y-direction velocity components, pressure and temperature, kinematic viscosity, density, thermal conductivity, electrical conductivity, volumetric expansion coefficient, and the rate of volumetric heat generation, specific heat capacity, respectively.

The initial and boundary values are defined in the following manner [30]:

For $t_0 = 0: \quad u = v = 0; \quad T = 0,\ 0 \le x \le H_E,\ 0 \le y \le H_E.$

For $t_0 > 0: \quad u = v = 0; \quad \dfrac{\partial T}{\partial y} = 0,\ y = 0$ and $y = H_E,$ (2.5)

$u = v = 0; \quad T = T_h, \quad$ at $\quad x = 0,\ 0 \le y \le \dfrac{H_E}{2}$ for bottom (B) source;

$\dfrac{H_E}{4} \le y \le \dfrac{H_E}{2}$ for middle (M) source; $\dfrac{H_E}{2} \le y \le H_E$ for top (T) source;

$u = v = 0; \quad T = T_c, \quad$ at $\quad x = H_E,\ 0 \le y \le \dfrac{H_E}{2}$ for bottom (B) sink;

$\dfrac{H_E}{4} \le y \le \dfrac{H_E}{2}$ for middle (M) sink; $\dfrac{H_E}{2} \le y \le H_E$ for top (T) sink;

$u = v = 0; \quad \dfrac{\partial T}{\partial x} = 0$, elsewhere on $x = 0$ and $x = H_E$.

The governing Eqs (2.1)-(2.4) and the imposed boundary values are changed to dimensionless procedure by using the non-dimensional quantities

$$X = \frac{x}{H_E}, \quad Y = \frac{y}{H_E}, \quad U = \frac{uH_E}{\upsilon}, \quad V = \frac{vH_E}{\upsilon}, \quad \tau = \frac{t_0 \upsilon}{{H_E}^2}, \quad \theta = \frac{T - T_c}{T_h - T_c}, \quad P = \frac{p{H_E}^2}{\rho} \tag{2.6}$$

and the following set of equations are obtained in the non-dimensional form as [11, 28, 27],

$$\frac{\partial U}{\partial X} + \frac{\partial V}{\partial Y} = 0, \tag{2.7}$$

$$\frac{\partial U}{\partial \tau} + U\frac{\partial U}{\partial X} + V\frac{\partial V}{\partial Y} = -\frac{\partial P}{\partial X} + \frac{\partial^2 U}{\partial X^2} + \frac{\partial^2 U}{\partial Y^2}, \tag{2.8}$$

$$\frac{\partial V}{\partial \tau} + U\frac{\partial V}{\partial X} + V\frac{\partial V}{\partial Y} = -\frac{\partial P}{\partial Y} + \frac{\partial^2 V}{\partial X^2} + \frac{\partial^2 V}{\partial Y^2} + Gr\left|\theta - \theta_m\right|^b - Ha^2 V, \tag{2.9}$$

$$\frac{\partial \theta}{\partial \tau} + U\frac{\partial \theta}{\partial X} + V\frac{\partial \theta}{\partial Y} = \frac{1}{Pr}\left[\frac{\partial^2 \theta}{\partial X^2} + \frac{\partial^2 \theta}{\partial Y^2}\right] + Q\theta \tag{2.10}$$

where, $Gr = \dfrac{g\beta\left|T - T_m\right|^b {H_E}^3}{\upsilon^2}$ is the modified Grashof number, $Ha = B_0 H_E \sqrt{\dfrac{\sigma_e}{\mu}}$ is the Hartmann number,

$Pr = \frac{\upsilon}{\alpha}$ is the Prandtl number, $\theta_m = \frac{T_m - T_c}{T_h - T_c}$ is the density inversion parameter, and $Q = \frac{q''' H_E^{\,2}}{\upsilon \rho_0 c_p}$ is the internal heat absorption/generation parameter.

The initial and boundary values are altered in the form as follows:

For $\tau = 0$: $U = V = 0, 0 \le X \le 1$ and $0 \le Y \le 1$.

For $\tau > 0$: $U = V = 0, \frac{\partial \theta}{\partial Y} = 0, Y = 0$ and $Y = 1$,

$U = V = 0, \theta = 1$ at $X = 0$, $0 \le Y \le \frac{1}{2}$ for bottom (B) source;

$\frac{1}{4} \le Y \le \frac{1}{2}$ for middle (M) source; $\frac{1}{2} \le Y \le 1$ for top (T) source.

$U = V = 0, \theta = 0$ at $X = 1, 0 \le Y \le \frac{1}{2}$ for bottom (B) sink;

$\frac{1}{4} \le Y \le \frac{1}{2}$ for middle (M) sink; $\frac{1}{2} \le Y \le 1$ for top (T) sink;

$U = V = 0, \frac{\partial \theta}{\partial X} = 0$ elsewhere.

The Nusselt number that calculates the rate of heat transmission across the cavity is measured by $Nu = -\frac{H_E}{k(T_h - T_c)} \frac{\partial T}{\partial x}$, and its dimensionless form across the left sidewall of cavity is defined as $Nu = -\left[\frac{\partial \theta}{\partial X}\right]_{X=0}$. The total heat transfer that is measured by averaged Nusselt number ($\overline{Nu}$) along the partial thermal walls and is defined by

$$\overline{Nu} = \frac{2}{H_E} \int_{h_H}^{\frac{H_E}{2} + h_H} Nu \, dY \tag{2.11}$$

where $h_H = \frac{H_E}{2}, \frac{H_E}{4}, 0$ for top, middle and bottom heating portions respectively. Consequently, numerical integration is accomplished for each time step for the calculation of $\overline{Nu}$.

3. Method of solution

To study the MHD convection inside the cavity, finite volume method is utilized to discretize the governing Eqs (2.7)-(2.10) combined with the boundary conditions. To discretize the convective term and diffusive term, QUICK scheme and central difference scheme, respectively, are used with a uniform grid size of 101×101. The time-step of 10^{-4} is chosen in the implicit scheme for time marching terms. The SIMPLE

algorithm connects the velocities and pressure. The subsequent set of equations from each unknown is solved by Gauss-Seidel iterative procedure. The repetition is continued until the convergence measure $\left|\frac{\phi_{n+1}(i,j)-\phi_n(i,j)}{\phi_{n+1}(i,j)}\right| \le 10^{-6}$ is achieved for each variable. Here, the subscript n symbolizes previous iteration and $n+1$ symbolizes the current level.

In a numerical investigation, it is an essential to validate the results from in-house code. The results attained from the (in-house) code are compared with the free convection in a closed chamber with partially (thermally) active walls stated in Valencia and Frederick [27] in order to determine the correctness and validity of the internal (ForTran 90) code for the current problem. The outcomes are displayed in the Tab.1. The table shows that the outcomes of the current simulation were in decent agreement with the findings of the earlier inquiry. It gives us the assurance that our numerical method will work as intended.

Table 1. Averaged Nusselt number comparison for several arrangement with $Tm = 0, Ha = 0$.

Rayleigh Number	Source-Sink Arrangement	$\overline{Nu}$	
		Valencia and Frederick [27]	Present
$Ra = 10^4$	Case 5 (TB)	*2.142*	*2.115*
$Ra = 10^4$	Case 2 (MM)	*3.399*	*3.329*
$Ra = 10^4$	Case 4 (BT)	*2.997*	*3.108*
$Ra = 10^6$	Case 5 (TB)	*4.505*	*4.427*
$Ra = 10^6$	Case 2 (MM)	*12.028*	*11.978*
$Ra = 10^6$	Case 4 (BT)	*11.659*	*11.527*

4. Results and discussion

The streamlines and isotherms are examined for different values of heat absorption/generation parameter that range between *–10* and *10* in the increment of *5* and the Hartmann number is kept as *25*. In the analysis, the sink-source locations are placed in different combinations; in particular, they are placed along the top portion of walls referred as case 1 (TT). The center locations are referred as case 2 (MM) and bottom arrangements referred as case 3 (BB). The source at bottom of left wall and sink at top of right all referred as case 4 (BT).

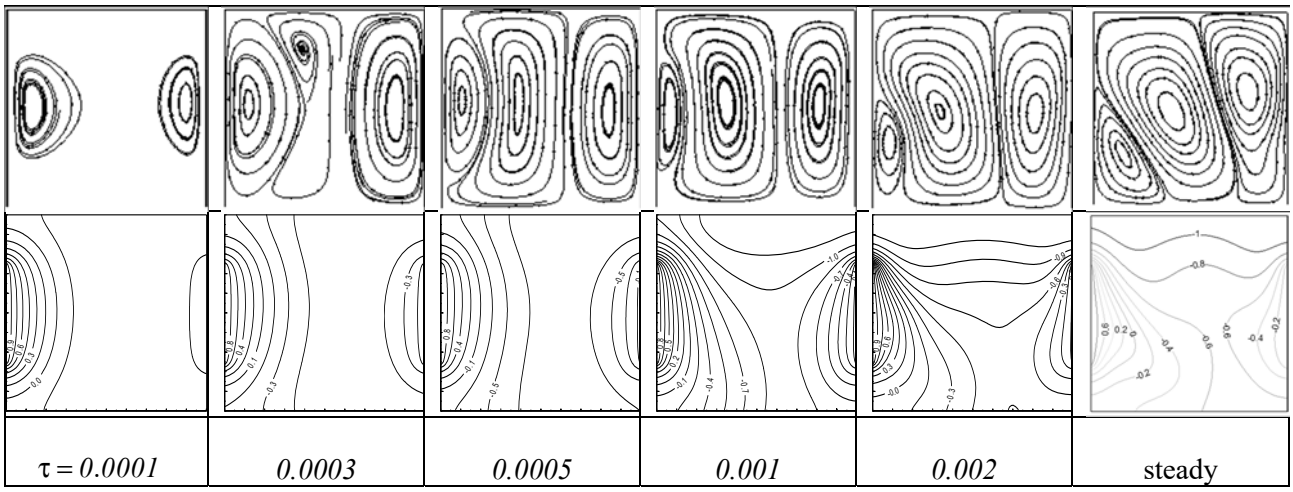

Fig.2. Transient state of flow field and isotherms for MM location, $Ha = 25,\ Q = -10$.

Similarly, the source at top of left wall and sink at bottom of right all referred as case 5 (TB). The main distinctiveness of this current study includes two important analyses: one the changes in stream pattern due to the variations of internal heat absorption/generation in the occurrence of (external) uniform magnetic field and the second is the corresponding variations in temperature due to the occurrence of heat source or heat sink inside the cavity. The calculations on the variations in local and averaged Nusselt number are performed and are presented in order for diverse values of internal heat absorption/generation and Hartmann number.

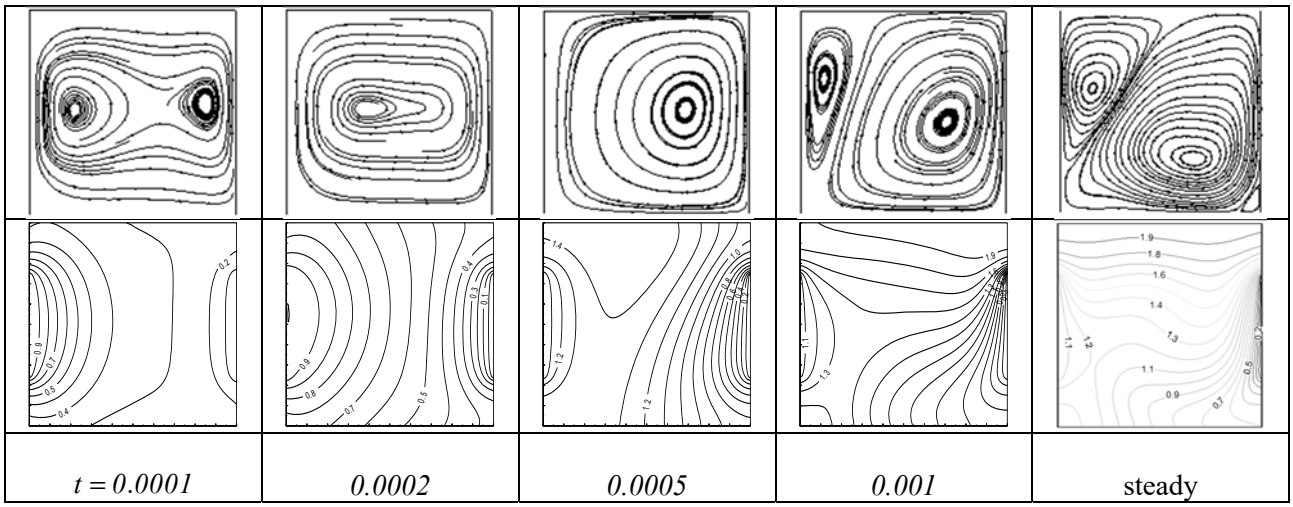

Fig.3. Transient state of flow field and isotherms for MM location, $Ha = 25,\ Q = 10$.

Figures 2 and 3 respectively show the transient behavior of flow field and isotherms for case 2 (MM) while $Ha = 25,\ -Q = 10$ and $Q = 10$. It is seen, for the absorption of heat, when $\tau = 0.0001$, the formation of multi-cells begins inside the cavity and over the time, flow pattern becomes steady. On viewing its isotherms, the lower portion of the chamber remain hotter than the cavity's upper portion. For both flow field and isotherms, the steady state prevails inside the cavity for $\tau > 0.002$. In the case of heat generation, that is, when $Q = 10$, the entire cavity remain hotter than its end temperatures and it is seen that the temperature of the upper part (of chamber) is higher than the lower region of the chamber. The change in flow and temperature becomes steady for $\tau > 0.001$.

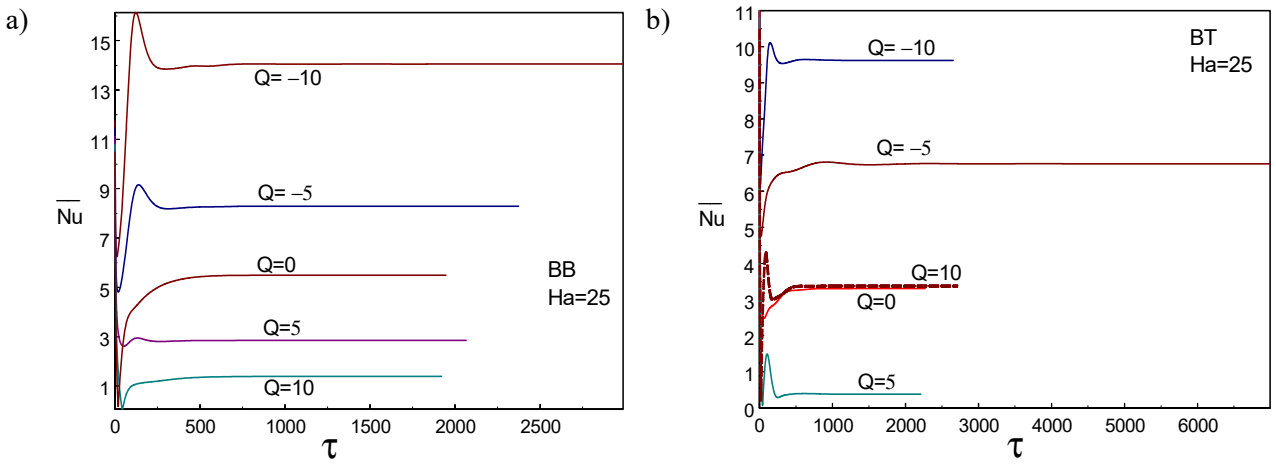

Fig.4. Time history of averaged Nusselt number for different Q and thermal locations.

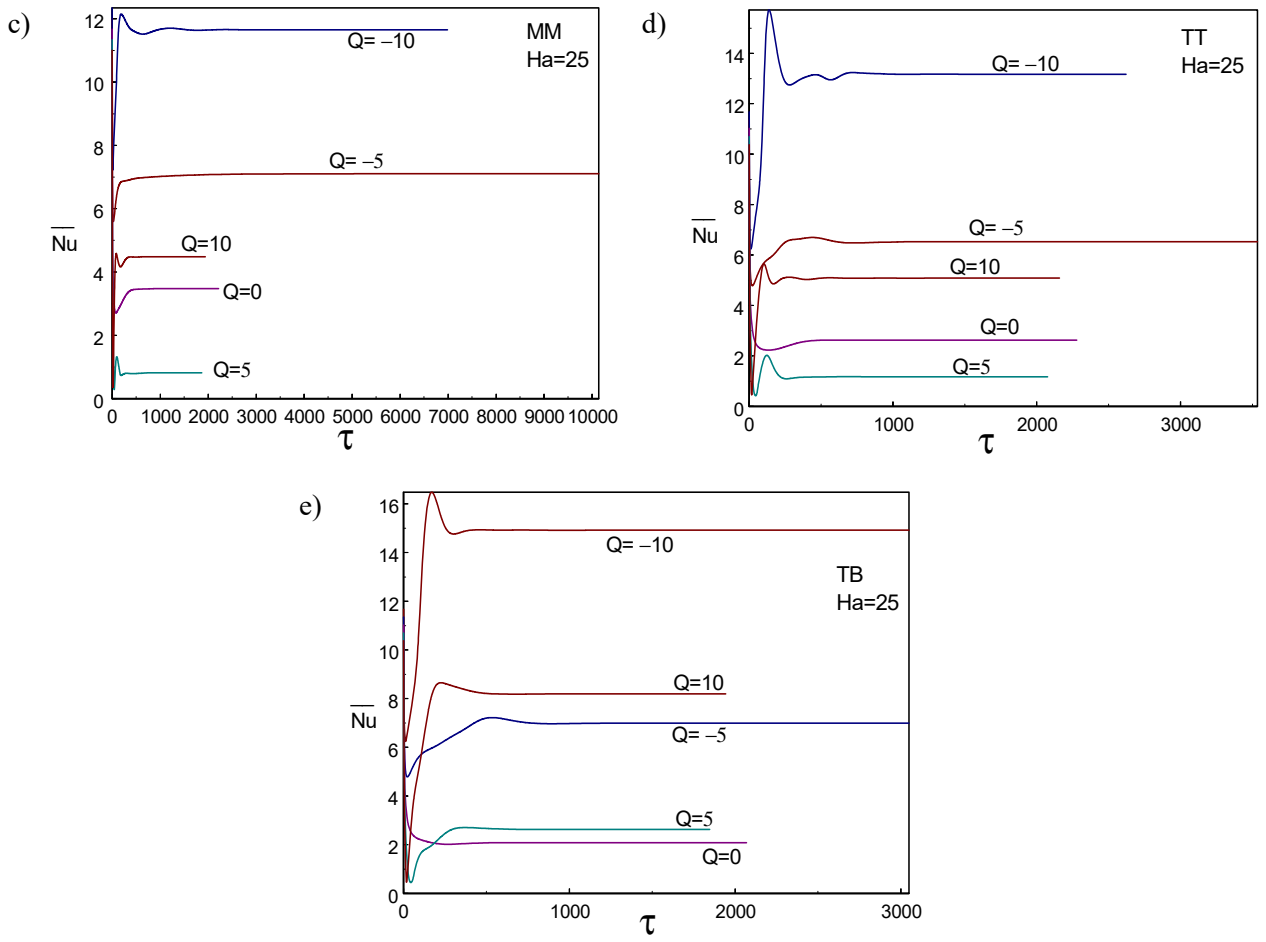

Fig.4 cont. Time history of averaged Nusselt number for different Q and thermal locations.

Figure 4(a)-(e) illustrates the time evaluations of averaged Nusselt number values for diverse internal heat generation parameter values when $Ha = 25$. On interpreting the results obtained for case 5 (TB), for $\tau > 0.001$, the transient behavior attains a steady state for both the heat generation and heat absorption scenario.

Figure 4 demonstrated the time history of the heat transfer rate for numerous values of heat generation parameter and source-sink pairs with $Ha = 25$. As time progresses, the liquid particle(s) close to the hot source gain higher amount of temperature and heat transference rate starts declining then get sudden fall and overshoot in the value of averaged Nusselt number as seen to be constant. The heat absorption takes more time to get the convergence (to reach the steady state) that heat generation case for all considered sink-source cases. When both sink and source are placed at bottom (case 3), the period to attain the steady state is less compared to other cases. The case 2 (MM) takes more time to approach the steady state condition. A small amount of internal heat generation will help the thermal mixing well and reaches quickly the steady state condition for all considered cases.

The analysis is made on the effect of varying internal heat absorption/generation under the occurrence of uniform magnetic field performing in the path similar to the horizontal axis. Figures 5 and 6 illustrate the resulting streamlines and temperature for diverse values of heat absorption/generation parameter Q and locations of thermal walls when $Ha = 25$. Specifically, the discussion is carried out for the internal heat generation values $-10,\ 0,\ 10$. When the internal heat generation is negative, it acts as a heat sink within the cavity due to the absorption of heat. On the other hand for heat generation, exothermic reaction takes place thus acting as a heat source. So, the temperature inside the cavity is more than the maintained boundary temperature. Also, the transfer rate depends on the development of several layered multi-cells in the chamber.

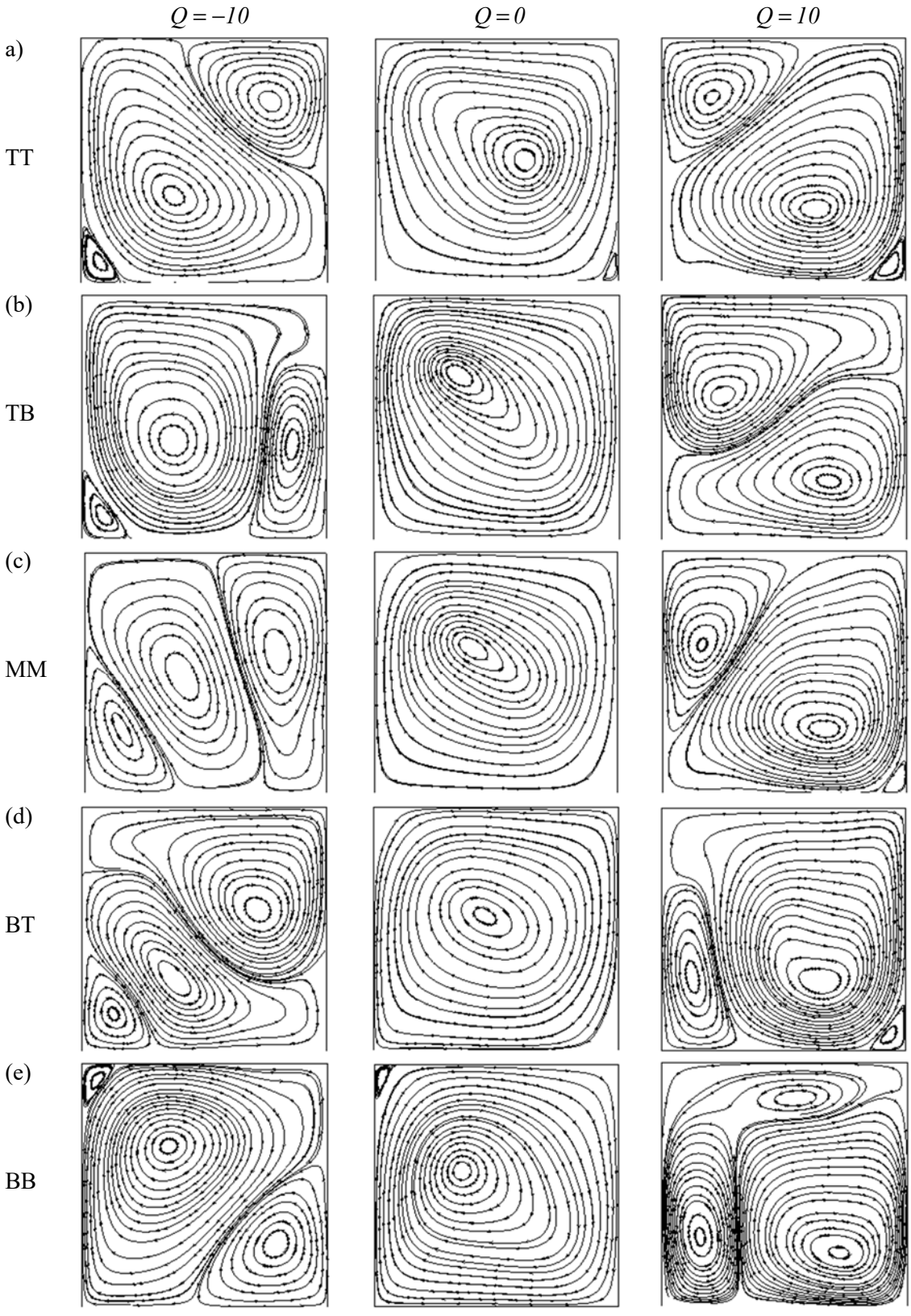

Fig.5. Streamlines for different heat generation parameters and locations with $Ha = 25$.

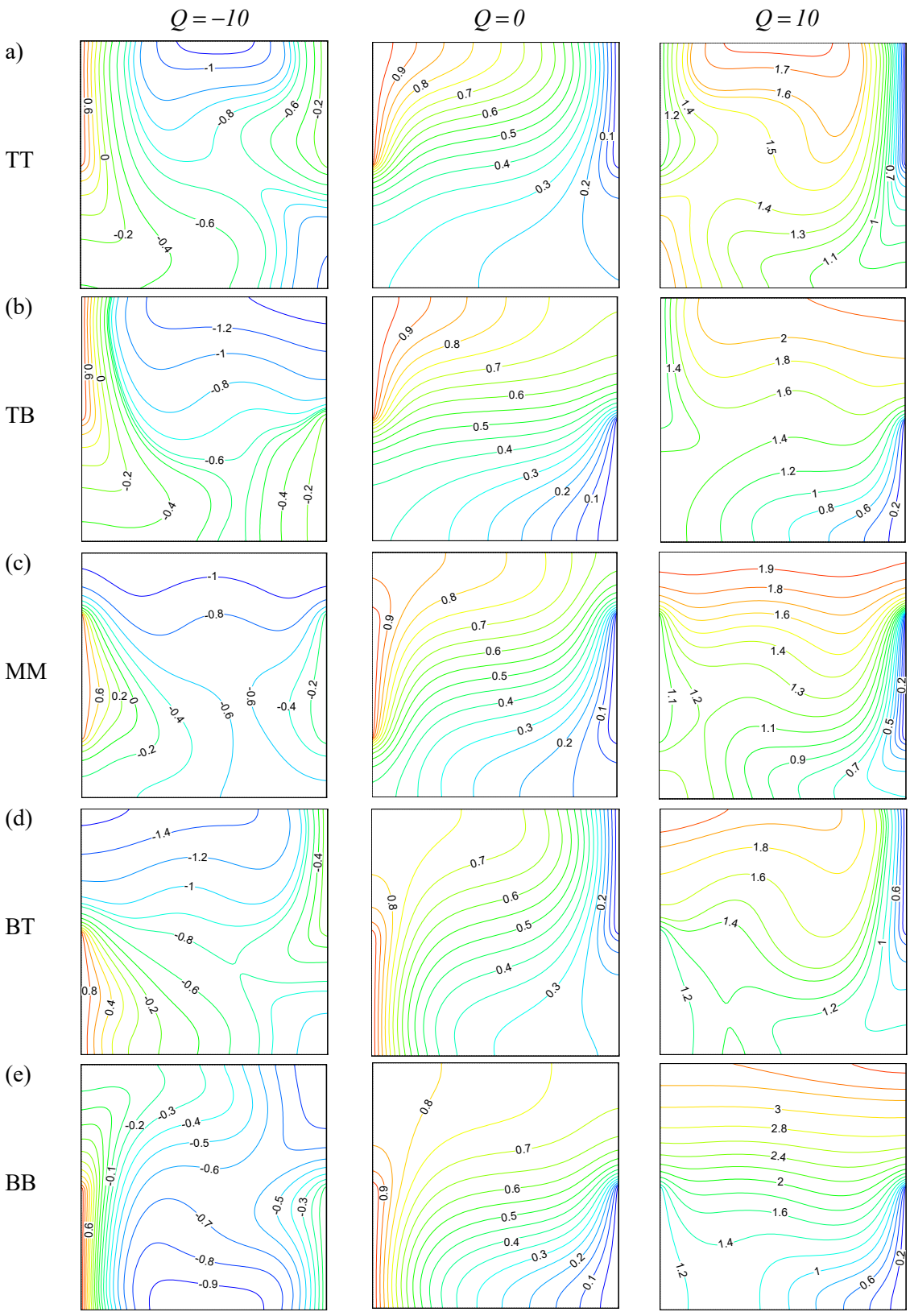

Fig.6. Isotherms for different heat generation parameters and locations with $Ha = 25$.

It can be perceived from the Fig.5(a) that multi-cells are molded inside the chamber for both internal heat generation and internal heat absorption cases while the active zones are placed in top-top position. When $Q = -10$, the stream comprises of a primary cell that occupies the majority of the cavity and a secondary cell shaped near the right-top corner of the chamber. On the other hand, when $Q = 10$, secondary cell elongates in the flow and occupies the chamber pushing the major cell to the left-top corner. When $Q = 0$, only single clockwise revolving eddy is formed inside the chamber occupying the entire space.

Figure 5(b) presents the formation of cells when the partially active wall locations are shifted to TM. Multi-cells are observed inside the cavity when the heat source and heat sinks are included to it. For the absorption case, the primary cell rotates in anticlockwise sense and secondary cell flows in clockwise direction. Here, the primary cell occupies majority of the enclosure. However, for heat generation case, dual cells are formed inside the cavity and they equally occupy the upper and the lower portion of the cavity. The flow about the upper portion is in counter clockwise sense and the flow about the lower portion is in clockwise sense. When there is no heat generation, single flow cell rotating in clockwise occurs inside the cavity. In the occurrence of heat generation and when the locations are altered to case 4 (BT), the flow becomes bi-cellular and the secondary cell suppresses the primary cell inside the cavity. It is shown in Fig.5(d). Inside the cavity, the secondary cell rotates anticlockwise and the primary cell rotates in clockwise sense. When internal heat generation is not present, the flow with single anticlockwise cell is observed there. When heat absorption happens, again multi-cells formations happen inside the cavity. In Fig.5(c) it is noted that in the flow pattern of case 2 (MM) position; multi-cells occupy the cavity for both heat absorption and heat generation cases. Anticlockwise rotating single cell take up the cavity in the nonappearance of heat generation. Figure 5(e) shows the active locations being altered to case 3 (BB) position. In this location, the presence of heat generation creates strong thermal layers along the left sidewall of the chamber. Whereas for heat absorption, clockwise rotating cell with weak thermal layers occupy the larger-area of the chamber. This primary cell pushes the minor cell to the right-bottom corner of the chamber. Finally, when there is no internal heat generation; single flow cell revolving in right-handed sense fills the entire domain.

Figure 6 illustrates the isotherms for different heat generation parameter and locations with $Ha = 25$. In the nonappearance of heat generation, the heat transfer inside the chamber takes place in a stratified manner when hot and cold walls are located in the case 1 (TT) spot (Fig.6(a)). In the occurrence of heat generation, cavity's temperature increases and this forms a thermal boundary layer close to the cold wall. When the heat generation value is reduced to negative value, that is, in the case of heat absorption, low temperature prevails in the upper portion of the cavity near the cold wall. Raise in temperature is observed close to hot wall of the cavity and the all the other parts of the cavity experience low temperature. Figure 6(b) displays the temperature distribution of top-bottom position of thermal walls. In this location, the occurrence of heat generation produces high temperature in the upper portion of the cavity when compared to lower portion of the cavity. When heat absorption is present in the case 5(TB) location, temperature in the lower part of the domain remains low. However, in the absence of internal heat generation, heat gradually transfers from the upper-left region of the cavity toward the lower-right, resulting in lower temperatures near the cold wall.

In the position case 2 (MM), while the heat generation is present, upper portion of the cavity uphold high temperature when compared to lower portion and on reducing the heat generation value to negative low temperature is observed there. It is also noted that the entire cavity remains hot in the existence of heat generation and in its absence the temperature gradually declines from the location of hot wall to cold wall. Graphical results for the case(MM) location are displayed in Fig.6(c).When the locations are placed in the case 4 (BT) part of the cavity, the temperature inside the cavity gets altered and high temperature values are viewed near the left-upper wall for positive heat generation value $Q = 10$. On the other hand when the value is decreased to negative the temperature inside the cavity also gets decreased showing very low temperature near the cold wall as seen in Fig.6(d). In the nonappearance of heat generation, temperature inside the cavity decreases as the fluid moves from hot region to the cold one. Due to buoyancy effect, the left-bottom part of the cavity shows high temperature and the top-right-corner of the chamber shows low temperature. Finally, in Fig.6(e), on examining the isotherms of case 3 (BB) location with heat absorption, formation of thermal boundary layers along the left wall near the thermal zone is observed. When internal heat generation value

increases positively, the temperature increases inside the cavity and the top part of the chamber is hotter when compared to the lower portion of the chamber. In the nonappearance of heat generation the left-side regime of the chamber is hotter than the right-side area of the domain and low temperature is observed near the cold wall.

Figure 7 demonstrates the local Nusselt number for various locations of thermal zones when $Ha = 25$ and $Gr = 10^6$. The graph represents the variations in heat transfer rate for different heat generation parameter values $-10, -5, 0, 5, 10$ including the combination of five locations. When the active locations are located in the case 1(TT) and case 5 (TB) positions, the heater is placed at the top of the left wall. Here the (local) Nusselt number value sharply decreases at the starting edge of the heater, gradually increases along the heater and then slightly decreases at the end of the heater. This effect is observed for the internal heat generation and absorption values -10 and 10. In the absence of heat generation, local Nusselt number decreases along with the heater. For case 2 (MM) position as shown in Fig.7(c), and with heat absorption or heat generation, the Nusselt number value decreases along with the heater and towards the edge of the heater a sharp increase in heat transfer is observed. However, when there is no heat generation, Nusselt number decreases along the position of the heater. Further monitoring the figures of case 4 (BT) and case 3 (BB) locations, local Nusselt number drastically increases nearby the heat source's upper edge in the presence of heat generation, specifically when $Q = 10$.

Figure 8 summarizes the overall heat transfer variations for diverse locations of active thermal sectors, different Hartmann number and fixed values of Grashof number 10^6. The graph depicts the total heat transference rates for diverse locations and internal heat generation parameter. When there is no magnetic field, i.e., $Ha = 0$, maximum heat transfer rate is noted while the thermal regions are positioned in the case 5 (TB) site for $Q = -10$, 5 and 10 and when $Q = -5$ and $Q = 0$, the overall heat transfer rate is more for the case 2 (MM) site. However, from the results, case 3 (BB) place shows a consistent heat transmission for all values of internal heat absorption/generation parameter. On varying Ha to 10, it is observed that the case 5 (TB) position gives high heat transfer rate for the values $Q = -10$, 5 and 10. In contrast, poor heat transfer is noted when $Q = 0$. Interesting observation is that, irrespective of variations in internal heat generation parameter, the amount of heat transmission seems to be consistent for all values of internal heat generation when the locations are shifted to down-down location. On rising the Hartmann number to 25, again high rate of heat transport is detected for case 5 (TB) position and for the values of internal heat generation -10, 5 and 10. But for this case, when the heat generation values are -5 and 0, low heat transfer rate is detected. Similarly, on analyzing the heat transmission rate for the position case 2 (MM), the outcome of heat transfer is considerably more for $Q = -10$ and for all other values of internal heat generation parameter, rate at which heat transfer takes place seems to be low. From the results obtained for case 4 (BT) location, it is noted that among the other locations of thermal zones, rate of heat transfer appears to be very less for all values of Q. However, it is viewed that case 3 (BB) position shows a least heat transfer for all deviations of internal heat absorption/generation parameter. When $Ha = 50$, case 4 (BT) and case 1 (TT) locations show poor heat transfer when compared to other thermal locations. Also, high heat transfer is witnessed for the case 5 (TB) position and lowest heat transmission is witnessed for case 3 (BB) position.

Figure 9 presents the bar chart that explains the comparison of heat transfer enhancement of various partially active walls with that of fully heated walls. The graph is plotted for heat transfer enhancement in percentage (E_{HT}) against the internal heat generation value Q for different Hartmann number values. The bar chart quantifies the amount of percent heat transmission increase that takes place inside the chamber when partially dynamic (thermal) walls are positioned along its lateral walls. Figure 9(a) depicts the heat transfer enhancement for BB location. When the thermally heated walls are placed on the case 3 (BB) part of the cavity and while $Q = 10$, enhanced heat transport takes place in the absence of magnetic field and when Ha is increased to 50, the heat transfer reduces from 275% to 150%. When $Q = -10$, rate of thermal energy transfer inside the chamber remain consistent and it is seen that at least 125% increase is seen for all Ha values. Figure 9(b) displays the heat transmission rate when the partial walls are sited along bottom-bottom location (case 3)

for diverse values of *Ha*. When $Q = 0$, poor heat transport takes place inside the cavity for all *Ha* values. When *Q* is increased to *10*, in the occurrence of magnetic field decreases the heat transport inside the cavity.

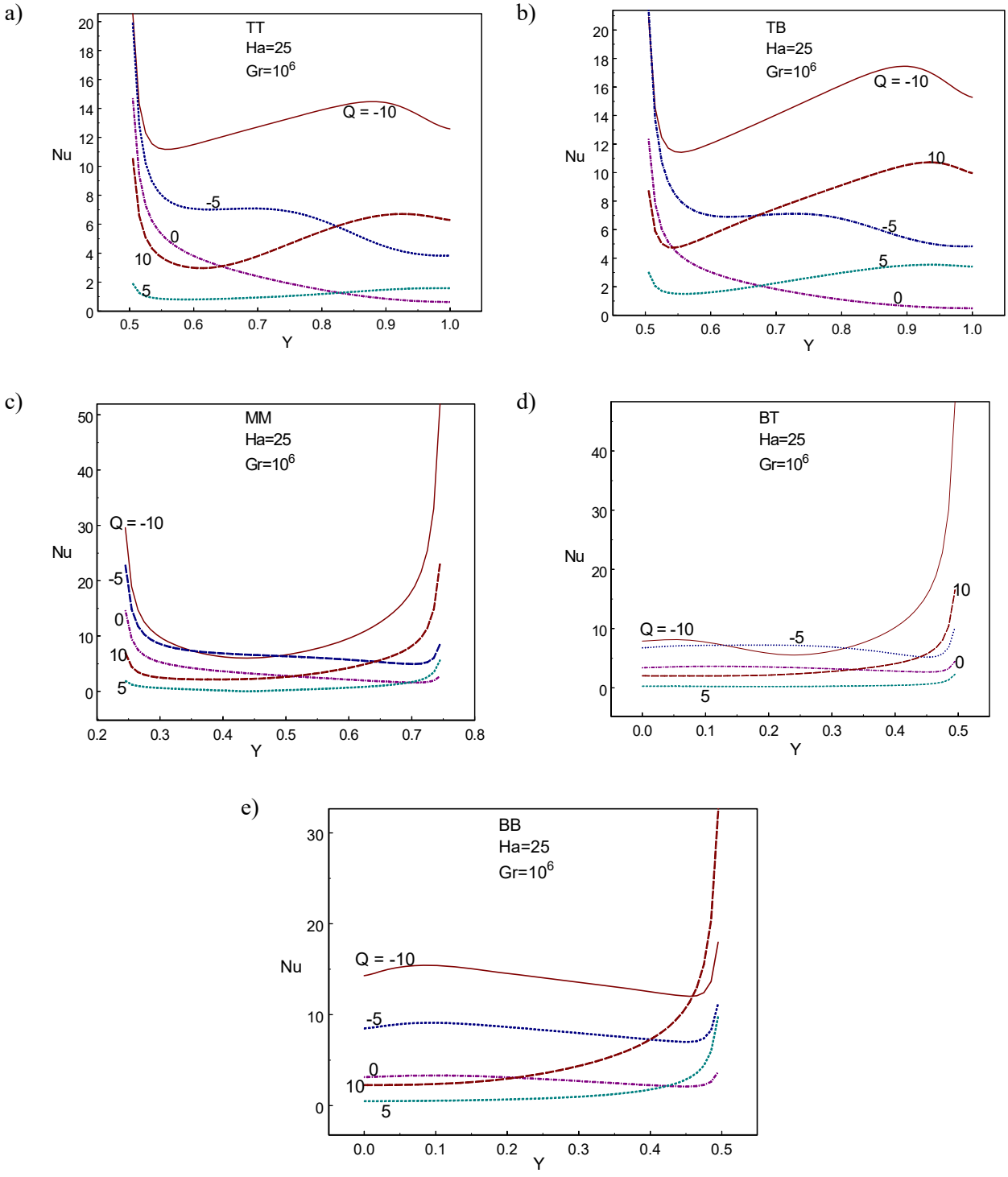

Fig.7. Local Nusselt number for different values of heat generation parameter

Figure 9(c) predicts numerically the amount of heat transport enhancement inside the chamber while the thermal zones are placed along middle-middle location. When $Q = -10, Ha = 0$, heat transport rate

enhances to *90%*. As the Hartmann value gets increased the heat transfer decreases by *10%*. For $Q = 0$, the rate of heat transmission seems high for $Ha = 50$. In contrast, when the heat generation value Q is increased to *10*, high heat transmission rate happens in the absence of magnetic field. The occurrence of magnetic field declines the heat transmission rate inside the cavity and it decreases by *80%*. However, compared to all other locations of partial walls, in the absence of internal heat generation, case 2 (MM) location shows enhanced heat transfer. Figure 9(d) illustrates numerically the heat transfer enhancement inside the chamber while the partial walls are sited in the case 1 (TT) location. When $Q = 0$, poor heat transmission takes place inside the chamber and while $Q = 10$ or $Q = -10$, enhanced heat transfer is witnessed inside the enclosure. It is again noted that the rise of *Ha* decreases the rate of heat transmission inside the chamber. Figure 9(e) portrays the results obtained for heat transfer enhancement when the partially thermally active walls are placed along top-bottom position. From the graph, it is vivid that high heat transfer rate is observed when the internal heat generation is present inside the cavity. That is, when *Q=10*, rate of transfer within the cavity is around *450%*. Though, the presence of magnetic field attenuates the heat transfer rate, while compared to all other heater/cooler locations, case 5 (TB) location shows enhanced heat transfer in the presence of internal heat generation. However, it is seen that in the presence of internal heat generation, the increase in the strength of magnetic field increase the heat transmission rate inside the chamber.

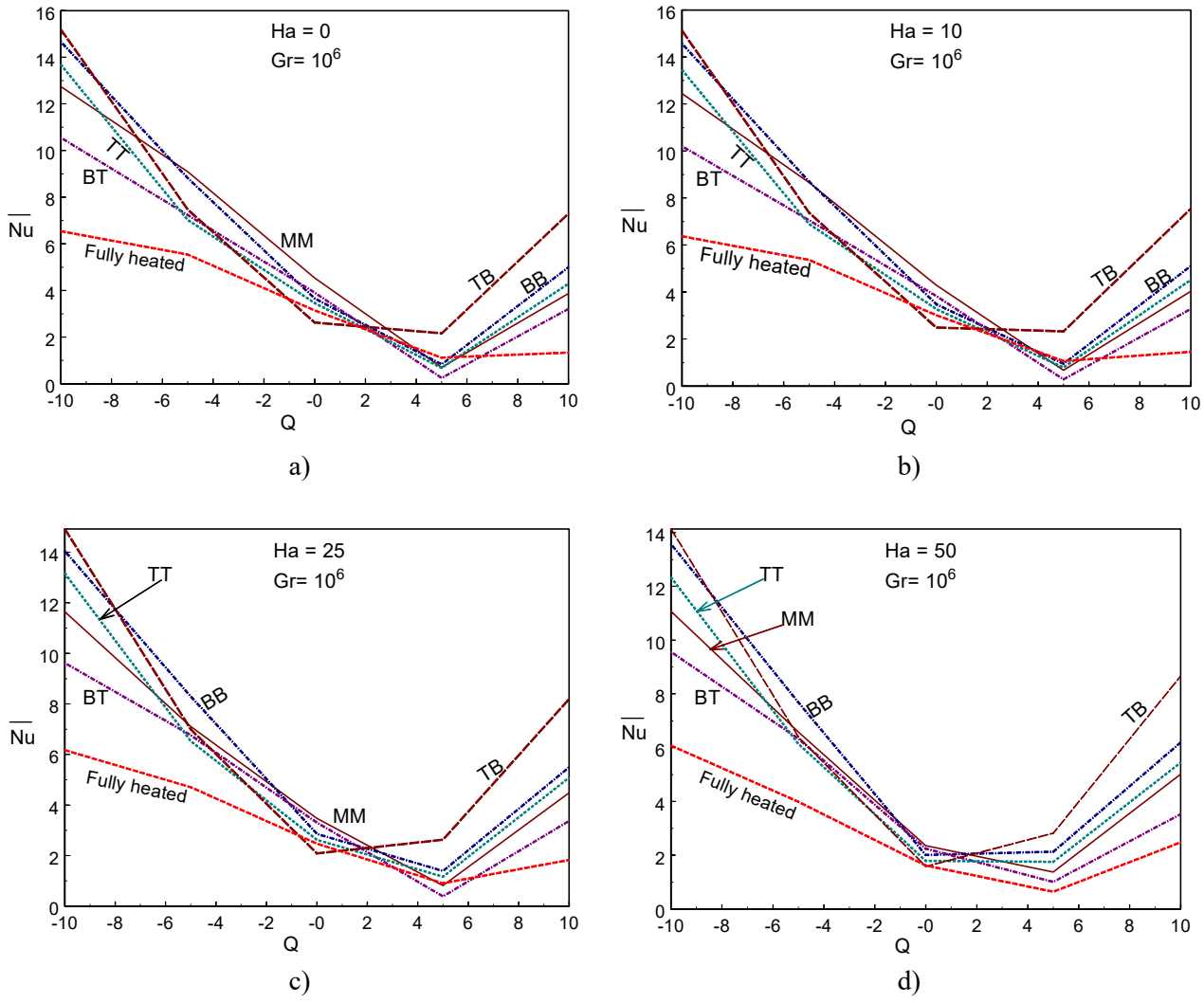

Fig.8. Average Nusselt number for different values of Hartmann number and heat generation parameter.

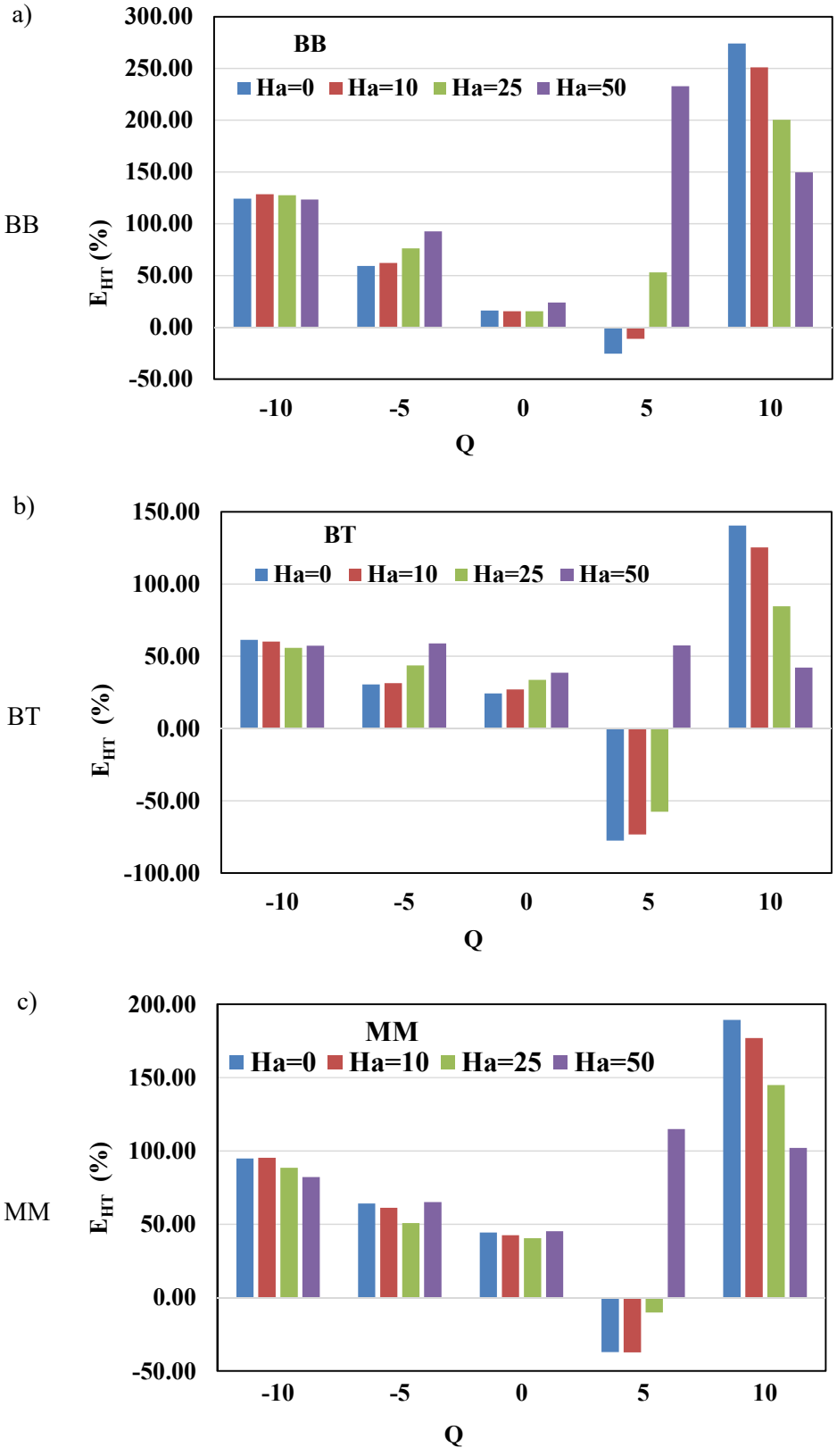

Fig.9. Heat transfer enhancement of various partially active thermal zones with fully heated wall.

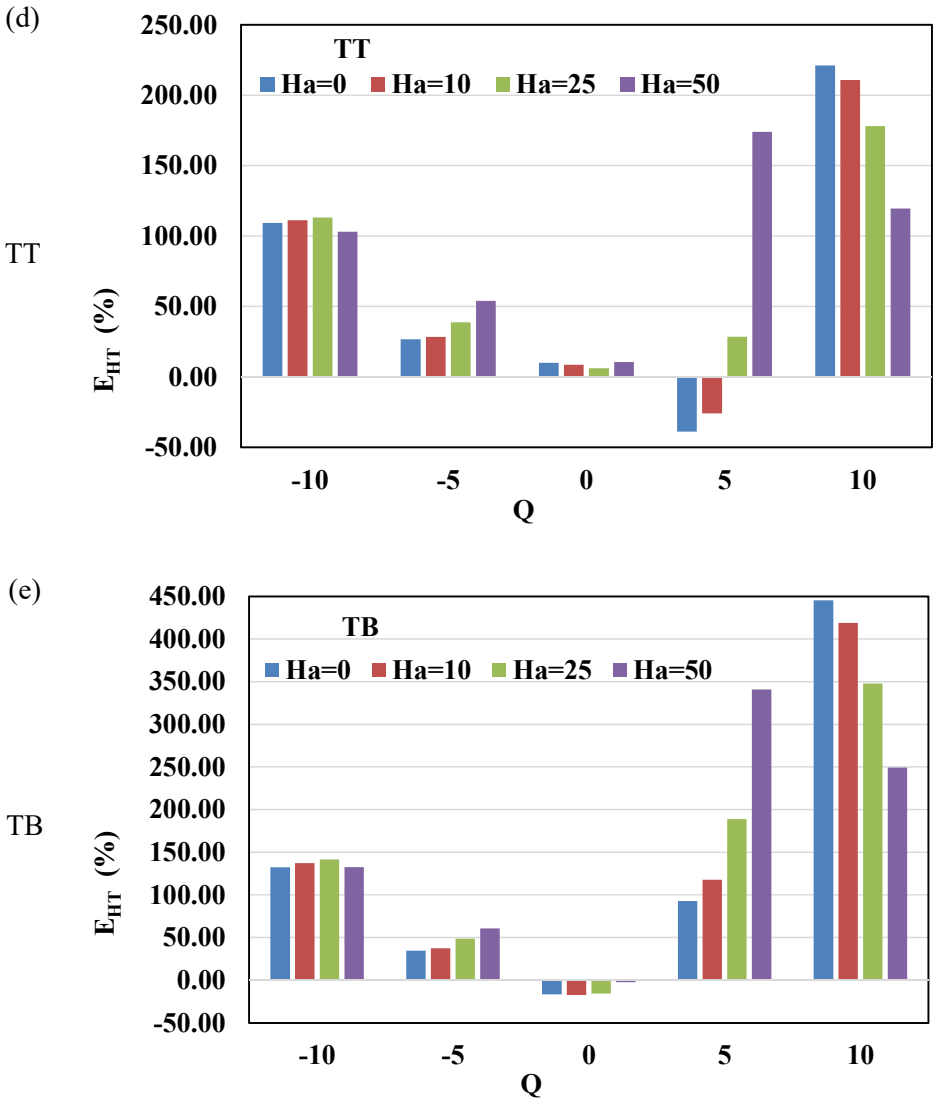

Fig.9 cont. Heat transfer enhancement of various partially active thermal zones with fully heated wall.

5. CONCLUSIONS

The impact of density inversion of cold water, sink-source arrangements and internal heat absorption/generation on MHD convection in a square chamber are analyzed for five different combinations of sink-source arrangements and for various values of internal heat absorption/generation parameter and Hartmann number. The following conclusions and remarks are made out of it:

- On varying the internal heat absorption/generation parameter, the stream pattern inside the cavity differs. Single cell flow pattern is observed in the nonappearance of heat absorption/generation and multi-cells occupy the chamber in the presence of absorption or generation.
- In the multi-cell formation, the primary cell occupies the majority area of the chamber for heat generation case and secondary cell dominates the cavity for heat absorption case.
- Convective heat transfer is high due to the creation of thermal boundary layer on placing the thermal zones either in the top-bottom or at the case 3, bottom-bottom locations.

- In the existence of heat absorption/generation, heat transport rate upsurges on decreasing the magnetic field's strength.
- In the absence of heat generation/absorption, center location of sink-source, Case 2 (MM), exhibits enhanced heat transfer.
- Out of the five cases analyzed, Case 5 (TB) demonstrated a higher transfer rate, while Case 4 (BT) exhibited a lower heat transmission rate in the presence of heat generation or absorption.
- The findings can be applied in industries such as electronic cooling devices, solar collectors, and thermal energy storage systems.

Nomenclature

B_o – magnetic field strength

c_p – specific heat

g – acceleration due to gravity

Gr – Grashof number

Ha – Hartmann number

H_E – height of the Enclosure $[m]$

k – thermal conductivity

Nu – local Nusselt number

$\overline{Nu}$ – average Nusselt number

P – pressure $\left[kg/m/s^2\right]$

Pr – Prandtl number

Q – heat generation parameter

q''' – heat generation rate

T – Temperature $[K]$

t_o – time

U,V – dimensionless velocity components

u,v – velocity components $[m/s]$

X,Y – dimensionless coordinates

x,y – Cartesian coordinates $[m]$

Greek symbols

β – coefficient of thermal expansion $\left[K^{-2}\right]$

ν – kinematic viscosity $\left[m^2/s\right]$

θ – dimensionless temperature

θ_m – density inversion parameter

ν – kinematic viscosity $\left[m^2/s\right]$

ρ_o – density $\left[kg/m^3\right]$

σ_e – electrical conductivity

τ – dimensionless time

Subscripts

c – cold

h – hot

m – maximum density

References

[1] Sid Ahmed A., Ayoub B., Najib B.M. and Manal B.A. (2024): *Conjugate mixed convection of a micropolar fluid over a vertical hollow circular cylinder*.– International Journal of Applied Mechanics and Engineering, vol.29, No.1, pp.1-18, https://doi.org/10.59441/ijame/181643.

[2] Saikia D.J. and Ahmed,N. (2023): *Impacts of chemical reaction, thermal radiation and heat source/sink on unsteady MHD natural convective flow through an oscillatory infinite vertical plate in porous medium*.– International Journal of Applied Mechanics and Engineering, vol.28, No.4, pp.114-136, https://doi.org/10.59441/ijame/174060.

[3] Palani G. and Arutchelvi A. (2023): *Similarity solution for MHD nanofluid flow with heat generation in the presence of radiation and chemical reaction effects*.– International Journal of Applied Mechanics and Engineering, vol.28, No.1, pp.71-83, https://doi.org/10.59441/ijame-2023-0007.

[4] Oni M. and Rilwan U. (2023). *Role of suction/injection on electromagnetohydrodynamics natural convection flow in a porous microchannel with electroosmotic effect*.– International Journal of Applied Mechanics and Engineering, vol.28, No.4, pp.94-113, https://doi.org/10.59441/ijame/173021.

[5] Touiker M., Bourouis A., Omara A. and Bouchair R. (2023): *Thermosolutal natural convection cooling process of a thermal source inside a partially porous cavity*.– International Journal of Computational Methods in Engineering Science and Mechanics, vol.24, No.3, pp.193-210, https://doi.org/10.1016/j.rinp.2021.103821.

[6] Rahimi A., Kasaeipoor A., Hasani Malekshah E. and Kolsi L. (2018): *Lattice Boltzmann simulation of free convection in nanofluid-filled cavity with partially active walls – entropy generation and heat line visualization*.– International Journal of Numerical Methods for Heat and Fluid Flow, vol.28, pp.2254-2283, https://doi.org/10.1108/HFF-06-2017-0229.

[7] Patterson J.C. (1984): *Unsteady natural convection in a cavity with internal heating and cooling*.– Journal of Fluid Mechanics, vol.40, pp.135-151, https://doi.org/10.1017/S0022112084000549.

[8] Baytas A.C. (1996): *Buoyancy driven flow in an enclosure containing time periodic internal sources*.– Journal of Heat and Mass Transfer, vol.31, pp.113-119.

[9] Tasaka Y. and Takeda Y. (2005): *Effects of heat source distribution on natural convection induced by internal heating*.– Int. Journal of Heat and Mass Transfer, vol.48, pp.1164-1174, https://doi.org/10.1016/j.ijheatmasstransfer.2004.09.044.

[10] Hossain M.A., Hafiz M.Z. and Rees D.A.S. (2005): *Buoyancy and thermo-capillary driven convection flow of an electrically conducting fluid in an enclosure with heat generation*.– International Journal of Thermal Sciences, vol.44, pp.676-684, https://doi.org/10.1016/j.ijthermalsci.2004.11.005.

[11] Saravanan S., Hakeem A.K.A., Kandaswamy P. and Lee J. (2008): *Buoyancy convection in a cavity with mutually orthogonal heated plates*.– Computers & Mathematics with Applications, vol.55, No.12, pp.2903-2912.

[12] Hakeem A.K.A., Saravana, S. and Kandaswamy P. (2008): *Buoyancy convection in a square cavity with mutually orthogonal heat generating baffles*.– International Journal of Heat and Fluid Flow, vol.29, No.4, pp.1164-1173.

[13] Ho C.J. and Tu F.J. (1999): *Numerical study on oscillatory convection of cold water in a tall vertical enclosure*.– Int. Journal of Numerical Methods for Heat and Fluid Flow, vol.9, pp.487-508, https://doi.org/10.1108/09615539910266639.

[14] Hossain M.A. and Rees D.A.S. (2005): *Natural convection flow of water near its density maximum in a rectangular enclosure having isothermal walls with heat generation*.– Heat and Mass Transfer, vol.41, pp.367-374, https://doi.org/10.1007/s00231-004-0551-3.

[15] Sivasankaran S. and Ho C.J. (2007): *Effect of temperature-dependent properties on MHD convection of water near its density maximum in a square cavity*.– International Journal of Thermal Sciences, vol.47, pp.1184-1194, https://doi.org/10.1016/j.ijthermalsci.2007.10.001.

[16] Oztop H.F., Nada E.A., Varol Y. and Chamka A. (2011): *Natural convection in wavy enclosures with volumetric heat sources*.– Int. Journal of Thermal Sciences, vol.50, pp.502-514, https://doi.org/10.1016/j.ijthermalsci.2010.10.015.

[17] Sahoo D.K. and Rathish Kumar B.V. (2024): *A variational multiscale stabilized finite element method for double diffusive incompressible flow with application to mixed convection in a heated staggered cavity under magnetic field*.– Int. J. of Comp. Methods in Engineering Science and Mechanics, Latest article, https://doi.org/10.1080/15502287.2024.2395996.

[18] Hiremath P., Hanumagowda B.N., Ananth Subray P.V., Sharma N., Varma S.V.K., Muhammad T. and Vinutha K. (2024): *Sensitivity analysis of MHD nanofluid flow in a composite permeable square enclosure with the corrugated wall using Response surface methodology-central composite design*.– Numerical Heat Transfer, Part A: Applications, pp.1-18, https://doi.org/10.1080/10407782.2024.2350029.

[19] Gangawane K.M. and Bharti R.P. (2018): *Computational analysis of magneto-hydrodynamic natural convection in partially differentially heated cavity: effect of cooler size*.– Proceedings of the Institution of Mechanical Engineers, Part C: Journal of Mechanical Engineering Science, vol.232, No.3, pp.515-528, https://doi.org/10.1177/0954406217752745.

[20] Bég O.A., Venkatadri K. and Prasad V. (2022): *Numerical study of magneto-hydrodynamic natural convection in a non-Darcian porous enclosure filled with electrically conducting helium gas*.– Proceedings of the Institution of Mechanical Engineers, Part C: Journal of Mechanical Engineering Science, vol.236, No.5, pp.2203-2223, https://doi.org/10.1177/0954406221100362410036624.

[21] Prasad K.V., Vajravelu K. and Vaidya H. (2016): *Hall effect on MHD flow and heat transfer over a stretching sheet with variable thickness*.– International Journal for Computational Methods in Engineering Science and Mechanics, vol.17, No.4, pp.288-297, https://doi.org/10.1080/15502287.2016.1209795.

[22] Joshi N., Upreti H. and Pandey A.K. (2022): *MHD Darcy-Forchheimer Cu-Ag/H2O-C2H6O2 hybrid nanofluid flow via a porous stretching sheet with suction/blowing and viscous dissipation*.– International Journal for Computational Methods in Engineering Science and Mechanics, vol.23, No.6, pp.527-535, https://doi.org/10.1080/15502287.2022.2030426.

[23] Saravanan S., Hakeem A.K.A. and Kandaswamy P. (2007): *Hydromagnetic natural convection in a partially heated cavity*.– International Journal of Heat and Technology, vol.25, pp.131-136.

[24] Sivasankaran S., Lee J. and Bhuvaneshwari M. (2011): *Effect of a partition on hydro-magnetic convection in an enclosure*.– *Arabian Journal for Science and Engineering*, vol.36, pp.1393-1406, https://doi.org/10.1007/s13369-011-0110-4.

[25] Sivasankaran S. and Bhuvaneswari M. (2011): *Effect of thermally active zones and direction of magnetic field on hydro magnetic convection in an enclosure*.– Thermal Science, vol.15, pp.367-382, https://doi.org/10.2298/TSCI100221094S.

[26] Malleswaran A., Sivasankaran S. and Bhuvaneswari M. (2013): *Effect of heating location and size on MHD mixed convection in a lid-driven cavity*.– International Journal of Numerical Methods for Heat and Fluid Flow, vol.23, pp.867-884, https://doi.org/10.1108/HFF-04-2011-0082.

[27] Benos L.Th., Kakarantzas S.C., Sarris I.E., Greco's A.P. and Vlachos N.S. (2014): *Analytical and numerical study of MHD natural convection in a horizontal shallow cavity with heat generation*.– International Journal of Heat and Mass Transfer, vol.75, pp.19-30, https://doi.org/10.1016/j.ijheatmasstransfer.2014.02.062.

[28] Janagi K., Sivasankaran S., Bhuvaneswari M. and Easwaramurthi M. (2016): *Numerical study on free convection of cold water in a square porous cavity heated with sinusoidal wall temperature*.– International Journal of Numerical Methods for Heat and Fluid Flow, vol.2, pp.1000-1014, https://doi.org/10.1108/HFF-10-2015-0453.

[29] Das D. and Basak T. (2017): *Analysis of entropy generation during natural convection in discretely heated porous square and triangular enclosures*.– Num. Heat Transfer, Part A: App., vol.71, pp.979-1003, https://doi.org/10.1080/10407782.2017.1326785.

[30] Valencia A. and Frederick R.L. (1989): *Heat transfer in square cavities with partially active thermal walls*.– International Journal of Heat and Mass Transfer, vol.32, pp.1564-1574, https://doi.org/10.1016/0017-9310(89)90078-1.

Received: February 23, 2025

Revised: September 10, 2025